Neurobiology of Aging 102 (2021) 111–118

Contents lists available at ScienceDirect

Neurobiology of Aging

journal homepage: www.elsevier.com/locate/neuaging.org

# Lower cerebral perfusion is associated with tau-PET in the entorhinal cortex across the Alzheimer's continuum

Anna Rubinski[a], Duygu Tosun[b], Nicolai Franzmeier[a], Julia Neitzel[a], Lukas Frontzkowski[a], Michael Weiner[b], Michael Ewers[a,c,*]

[a] Institute for Stroke and Dementia Research, Klinikum der Universität München, Ludwig-Maximilians-Universität LMU, Munich, Germany
[b] Department of Radiology and Biomedical Imaging, University of California, San Francisco, USA
[c] German Center for Neurodegenerative Diseases, Munich, Germany

ARTICLE INFO

*Article history:*
Received 22 September 2020
Revised 1 February 2021
Accepted 4 February 2021
Available online 10 February 2021

*Keywords:*
Alzheimer's Disease (AD)
Tau-PET
Amyloid-PET
Arterial Spin Labeling (ASL)
Cerebral Blood Flow (CBF)

ABSTRACT

Alzheimer's disease (AD) is associated with reduced temporo-parietal cerebral blood flow (CBF). However, a substantial variability in CBF across the clinical spectrum of AD has been reported, possibly due to differences in primary AD pathologies. Here, we assessed CBF (ASL-MRI), tau (AV1451-PET) and amyloid (AV45/FBB-PET) in 156 subjects across the AD continuum. Using mixed-effect regression analyses, we assessed the local associations between amyloid-PET, tau-PET and CBF in a hypothesis-driven way focusing on each pathology's predilection areas. The contribution of Apolipoprotein E (APOE) genotype, and MRI markers of small vessel disease (SVD) to alterations in CBF were assessed as well. Tau-PET was associated with lower CBF in the entorhinal cortex, independent of A$\beta$. Amyloid-PET was associated with lower CBF in temporo-parietal regions. No associations between MRI markers of SVD and CBF were observed. These results provide evidence that in addition to A$\beta$, pathologic tau is a major correlate of CBF in early Braak stages, independent of A$\beta$, APOE genotype and SVD markers.



## 1. Introduction

Reduced perfusion of the brain tissue is a common pathological alteration in Alzheimer's disease (AD) (Love and Miners, 2016). Alterations in perfusion, including lower cerebral blood flow (CBF), are predictive of cognitive decline (Xekardaki et al., 2015) and the conversion from mild cognitive impairment (MCI) to AD (Chao et al., 2010), rendering CBF measurement as a candidate biomarker of dementia risk (Wolters et al., 2017). CBF can be quantified using an arterial spin labeling (ASL) MRI sequence which uses magnetically labeled endogenous arterial blood water as a tracer (Wolf and Detre, 2007). Therefore, it provides a radiation free and noninvasive measure of CBF, and thus a clinically attractive alternative over radioactive tracers (Chen et al., 2011; Tosun et al., 2016).

Despite CBF alterations being common in AD, their link to primary pathologies including A$\beta$ and fibrillar tau remains unclear. Previously, a correlation between higher amyloid-PET and lower CBF was demonstrated across the spectrum of sporadic AD (Mattsson et al., 2014; Tosun et al., 2014) and autosomal dominant AD (McDade et al., 2014). However, no significant CBF reductions were observed in nondemented elderly who had abnormal CSF A$\beta_{1\text{-}42}$ yet normal CSF t-tau (Binnewijzend et al., 2016). Accumulating evidence shows that CSF tau proteins are associated with lower CBF in cognitively normal (CN) individuals (Stomrud et al., 2012) as well as in patients with MCI and AD dementia (Habert et al., 2010). These in vivo findings are corroborated by brain autopsy studies reporting that antemortem CBF reduction in AD is related to higher postmortem Braak stages of tau pathology (Bradley et al., 2002). However, neither postmortem histochemical analyses nor CSF biomarker studies allow for assessing region-specific effects of tau pathology on CBF. Moreover, given that A$\beta$ deposition is a strong predictor of tau accumulation (Jack et al., 2018), any association between tau and CBF may be related to A$\beta$ deposition. Therefore, the main focus of the current study was to test whether local tau-PET is associated with lower CBF in spatially corresponding brain regions, with and without controlling for the contribution of A$\beta$.

* Corresponding author at: Institute for Stroke and Dementia Research (ISD), Klinikum der Universität München, Feodor-Lynen-Straße 17, D-81377 Munich, Germany, Tel: +49 (0)89 4400 - 461221; fax: +49 (0)89 4400 – 46000.
*E-mail address:* Michael.Ewers@med.uni-muenchen.de (M. Ewers).

0197-4580/$ – see front matter © 2021 Elsevier Inc. All rights reserved.
https://doi.org/10.1016/j.neurobiolaging.2021.02.003

Here, we examined the regional associations between CBF (pseudo-continues ASL; pCASL), fibrillar tau ([$^{18}$F]AV1451-PET) and A$\beta$ ([$^{18}$F]AV45/([$^{18}$F]FBB-PET) in spatially matched regions of interest (ROIs). We restricted these ROI analyses in a hypothesis-driven manner to each pathology's predilection areas, that is, Braak-stage ROIs for tau-PET, and the default-mode-network (DMN) ROIs for amyloid-PET.

Furthermore, small vessel disease (SVD) is common both in aging and AD. Previous studies have shown that MRI proxies of SVD, namely, higher number of microbleeds (Gregg et al., 2015) and higher white matter hyperintensity (WMH) volume (Shi et al., 2016; Kim et al., 2020) are associated with reduced CBF. Since increased tau-PET levels are also observed in subjects with SVD (Kim et al., 2018), it is possible that any associations between tau and CBF are mediated by SVD.

Therefore, we assessed the contribution of markers of SVD including WMH and cerebral microbleeds in addition to tau-PET and amyloid-PET as predictors of CBF.

## 2. Methods

### 2.1. Participants

We included a sample of 156 participants comprised of CN (n = 84), amnestic MCI (n = 51) and AD dementia (n = 21) which were assessed at a total of 14 study sites within the Alzheimer's Disease Neuroimaging Initiative (ADNI; recruitment phase III). Beyond the inclusion criteria of ADNI, additional requirements comprised availability of 3D pCASL images and [$^{18}$F]AV1451 tau-PET obtained no longer than 12 months apart (mean 30.72 ± 39.78 days apart). In addition, 145 participants had either [$^{18}$F]AV45 amyloid-PET (n = 82) or [$^{18}$F]FBB amyloid-PET (n = 63) scans acquired within 12 months from the pCASL scan (mean 76.41 ± 115.32 days apart). Apolipoprotein E (APOE) genotyping was available in a subset of 140 participants.

The diagnostic criteria of CN in ADNI included a Mini Mental State Exanimation (MMSE) score ≥ 24, Clinical Dementia Rating (CDR) = 0 and no memory concerns (Petersen et al., 2010). Amnestic MCI participants had MMSE score ≥ 24, CDR = 0.5, subjective memory concern, objective memory loss measured by education adjusted scores on the Wechsler Memory Scale Memory II, absence of significant levels of impairment in other cognitive domains, essentially preserved activities of daily living and an absence of dementia (Petersen et al., 2010). AD dementia participants had MMSE score ≤ 26, CDR > 0.5 and fulfillment of NINCDS/ADRDA criteria for probable Alzheimer's disease (Petersen et al., 2010).

Ethical approval was obtained by the ADNI investigators, all participants provided written informed consent (further information about the inclusion/exclusion criteria may be found at www.adni-info.org).

### 2.2. T1 acquisition and preprocessing

All imaging data were downloaded from the ADNI LONI image archive (https://ida.loni.usc.edu). All MRI data were obtained on 3T General Electric (GE) MRI scanner according to standardized protocol within ADNI phase III. 3D T1-weighted scans were acquired using an accelerated Fast Spoiled Gradient Echo with Inversion Recovery-Preparation (IR-FSPGR) sequence, 1 mm isotropic resolution and a TR/TE/Flip angle = 7.3–7.7 s/3.05–3.12 ms/11°.

For each participant, we applied volumetric segmentation to the native-space structural images using FreeSurfer-based pipeline (version 6.0; freesurfer.net), in which subcortical and cortical areas are segmented automatically using the probabilistic Desikan-Killiany atlas (Desikan et al., 2006).

### 2.3. ASL acquisition and preprocessing

ASL-MRI scans were acquired using a 3D pCASL sequence on exclusively GE scanners with resolution = 1.9 × 1.9 × 4 mm$^3$ and a TR/TE/Flip angle = 4.9 s/10.5–10.7 ms/111°. ASL images were preprocessed with ExploreASL, an automated MATLAB based toolbox for ASL analysis (Mutsaerts et al., 2020). Quantitative CBF images were estimated based on recommended modeling for clinical applications (Alsop et al., 2015). The major assumptions of this model included homogeneous blood/brain partition coefficient of 0.9 mL/g for water, labeling inversion efficiency of 80%, background suppression efficiency of 75% and T1 of blood at 1.6 s. The partial saturation of the reference proton density image was corrected for by using a T1t of 1.2 s, typical of GM. The difference between the corrected proton density image and the perfusion weighted image, yielding the quantitative CBF in mL/100 g/min units of arterial water density. Partial volume effect (PVE) correction was performed using a spatial linear regression algorithm to estimate the flow contribution of each tissue at a given voxel as described previously (Asllani et al., 2008; Petr et al., 2018). All statistical analyses were computed based on PVE corrected CBF data.

PVE corrected CBF images in the participant's T1 space were resliced using SPM12 (Wellcome Trust Centre for Neuroimaging, University College London) to T1 resolution and ROI based values were extracted based on FreeSurfer anatomical parcellations from the T1 images. Regional CBF values were residualized by the mean signal of the precentral gyrus as the reference region in order to render comparability to earlier studies on the associations between amyloid-PET and ASL assessed CBF (Mattsson et al., 2014; Yew et al., 2017).

### 2.4. [18F]AV1451 tau-PET and [$^{18}$F]AV45/[$^{18}$F]FBB amyloid-PET acquisition and preprocessing

Tau-PET data were acquired for 30 minutes dynamic emission scan, six 5-minutes frames, 75105 minutes postinjection of 10.0 mCi of [$^{18}$F]AV1451. Amyloid-PET data were acquired for 20 minutes dynamic emission scan, four 5-minutes frames, 50–70 minutes post injection of 10.0 mCi of [$^{18}$F]AV45 or 20 minutes dynamic scan, four 5-minutes frames, 90–110 minutes post injection of 8.1 mCi of [$^{18}$F]FBB.

Final datasets including amyloid-PET and tau-PET ROI values were downloaded from the ADNI website. PET quality control and preprocessing were centrally conducted at the ADNI PET core center at University of California Berkeley as previously described (Jagust et al., 2015). The preprocessing steps included frame coregistration, averaging across the dynamic range and standardization with respect to the orientation, voxel size and intensity and smoothing to produce images of a uniform isotropic resolution of 8 mm FWHM (Jagust et al., 2015). Tau-PET scans were corrected for partial volume effects using the Geometric Transfer Matrix approach as previously described (Baker et al., 2017). Preprocessed PET images were subsequently coregistered to the participant's T1 image in native-space and FreeSurfer-based anatomical parcellations were applied to extract ROI based values. Standardized uptake value ratio (SUVR) scores were obtained by normalizing ROI values to the mean uptake of the whole cerebellum for amyloid-PET data, and to the mean uptake of the inferior cerebellar GM for tau-PET data, following previous recommendations (Landau et al., 2012; Maass et al., 2017).

### 2.5. Assessment of amyloid status

82 participant underwent [$^{18}$F]AV45 amyloid-PET and 63 participants [$^{18}$F]FBB amyloid PET. Amyloid status was computed fol-

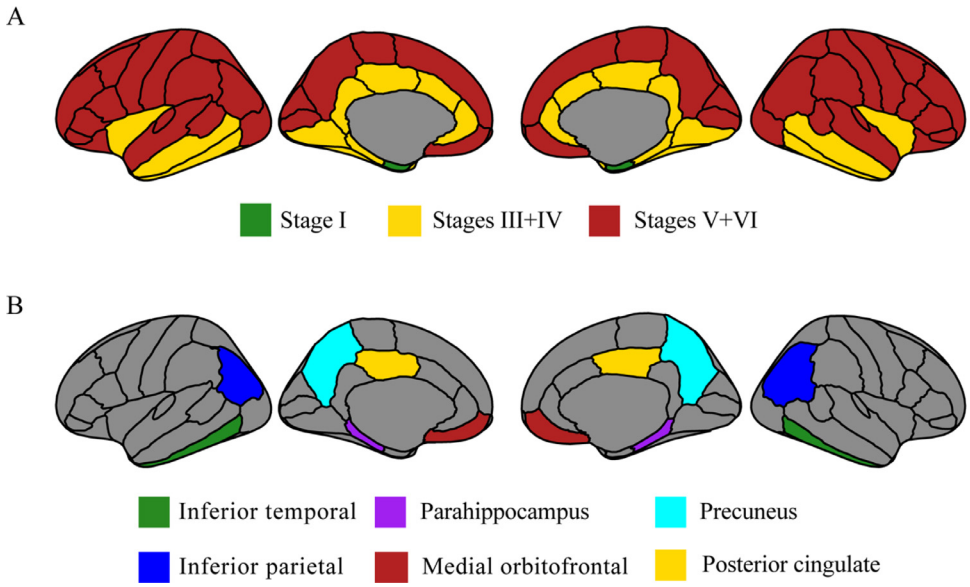


**Fig. 1.** (A) Spatial mapping of Braak stage-specific ROIs that were used to determine regional CBF and tau-PET uptake. For Braak stage II, the hippocampus was not included due to known off-target binding of the AV1451-PET tracer in that region. (B) Spatial mapping of default mode network ROIs that were used to determine regional CBF and amyloid-PET uptake.

lowing a method described previously (Landau et al., 2012). Briefly, the global cortical amyloid scores were calculated as a mean across FreeSurfer-derived cortical GM ROIs (frontal, lateral temporal, lateral parietal and anterior/posterior cingulate) divided by whole cerebellum reference region. Participants were classified as A$\beta$+ or A$\beta$- based on established cutoff values (global AV45-PET SUVR > 1.11 or global FBB-PET SUVR > 1.08) (Landau et al., 2012). To obtain comparable quantification of the amyloid burden across tracers, we used the following centiloid calculation as recommended for the ADNI pipeline: AV45 centiloid = 196.9 X $SUVR_{FBP}$ - 196.03, where $SUVR_{FBP}$ is the SUVR of AV45, and FBB centiloid = 159.08 X $SUVR_{FBB}$ − 151.65, where $SUVR_{FBB}$ is the SUVR of FBB).

### 2.6. A priori selection of ROIs

In order to test the association between tau-PET and CBF, we included ROIs defined by the Braak-staging (Fig. 1A). That is, average values for three composite ROIs scores including Braak stage I (entorhinal), Braak III/IV (limbic) and Braak V/VI (neocortical) were obtained for each modality including tau-PET, amyloid-PET and CBF. Braak stage II (hippocampus) was not included due to spill of from known off-target binding of the tau-PET tracer to choroid plexus (Marquie et al., 2015).

In order to test the association between amyloid-PET and CBF, we focused on DMN regions which are predilection areas of amyloid deposition early in the course of AD (Palmqvist et al., 2017). Values of amyloid-PET, tau-PET and CBF were extracted for 6 a priori designated ROIs within the DMN: medial-orbitofrontal, precuneus, posterior cingulate, inferior parietal, inferior temporal and parahippocampal gyrus (Fig. 1B). To obtain comparable quantification of the amyloid burden across tracers, we used the centiloid calculation mentioned above for regional amyloid-PET measures.

### 2.7. White matter hyperintensity segmentation

WMH volumes were extracted using T1 and Fluid-Attenuated Inversion Recovery (FLAIR) scans. 3D FLAIR scans were acquired with resolution = 1 × 1 × 1.2 $mm^3$ and a TR/TE/Flip angle = 4.8 s/119 ms/90°. Detailed information describing the assessment process is available online on the ADNI website (http://adni.loni.usc.edu/methods). The total WMH volume was divided by the total intracranial volume to obtain a normalized global WMH volume. Since WMHs typically have a skewed distribution, we applied an inverse-hyperbolic sine (IHS) transform to the WMH volume ratio, as reported previously (Caballero et al., 2020).

### 2.8. Cerebral microbleeds assessment

Cerebral microbleeds were defined as areas of signal void on T2*-weighted MRI and performed by ADNI MRI-Core (available for a subset of 155 participants). T2*-weighted scans were acquired with resolution = 0.85 × 0.85 × 4 $mm^3$ and a TR/TE/Flip angle = 650ms/20ms/20°. Relevant findings were cataloged with information about each observation of the finding on the associated T2* image. Findings cataloged as definite microbleeds were counted and used for further analysis. Detailed information describing the assessment process is available online on the ADNI website (http://adni.loni.usc.edu/methods).

### 2.9. Statistical analysis

Group demographics were compared between groups using Kruskal-Wallis for continuous measures (followed by Bonferroni-corrected post-hoc Dunn tests) and Chi-squared tests for categorical measures.

For all subsequent analysis on CBF, PVE-corrected values were used and for the sake of simplicity, we simply refer to CBF values. For our main analyses, we tested whether increased tau-PET was associated with reduced perfusion in Braak stage ROIs. To this end, we conducted mixed-effect regression analysis to test whether regional tau-PET levels are a significant predictor of participants' CBF in the 3 spatially matched composite Braak-stage ROIs, accounting for age, gender, diagnosis, education (fixed effects) and the study site as a random effect. Analyses were performed in the entire sample as well as in the nondemented subgroup (excluding AD dementia participants) or in subgroups defined by A$\beta$ status. Division

**Table 1**
Sample characteristics, mean (SD)

| Group | CN (n = 84) | MCI (n = 51) | AD (n = 21) | *p*-value |
|---|---|---|---|---|
| Age (years) | 72.70 (6.49) | 74.90 (8.05) | 76.10 (6.16) | 0.032 |
| Gender (M / F) | 36/48 | 31/20 | 14/7 | 0.045 |
| Education (years) | 16.71 (2.43) | 16.65 (2.59) | 15.76 (2.39) | 0.199 |
| MMSE | 29.35 (0.88) | 27.94 (2.41)* | 22.38 (3.81)*,† | <0.001 |
| Aβ-/Aβ+[a] | 55-/25+ | 32-/15+ | 18+*,† | <0.001 |
| APOE ε4 carriers -/+ [b] | 52-/30+ | 27-/15+ | 4-/12+*,† | 0.012 |
| Global Aβ centiloid [a] | 2.43 (28.65) | 28.34 (45.88) | 86.18 (31.39) *,† | <0.001 |
| Global tau-PET SUVR | 1.42 (0.15) | 1.52 (0.33) | 1.95 (0.95) *,† | <0.001 |
| Global GM CBF [c] (mL/100g/min) | 42.39 (9.73) | 38.25 (10.38) | 33.70 (12.31)* | <0.001 |
| WMH volume (mL) [d] | 3.13 (4.90) | 4.28 (4.73) | 6.22 (8.33)* | 0.003 |
| Microbleeds count [e] | 0.45 (0.89) | 0.75 (2.29) | 0.57 (0.81) | 0.604 |

Key: Aβ, amyloid-beta; AD, Alzheimer's disease; APOE, Apolipoprotein E; CBF, cerebral blood flow; CN, cognitively normal; F, female; GM, grey matter; M, male; MCI, mild cognitive impairment; MMSE, Mini-Mental State Exam; WMH, white matter hyperintensity.
* Significantly different from CN.
† Significantly different from MCI. (Significant after applying a Bonferroni-corrected α-threshold of 0.017).
[a] Available for 145 subjects.
[b] Available for 140 subjects.
[c] Data is PVE corrected.
[d] Raw, nontransformed data
[e] Available for 155 subjects.

to subgroups was performed in order to ensure that our results are not driven by extreme AD dementia cases or by Aβ burden.

Moreover, we checked whether there were few highly influential cases based on by Cook's distance D (Cook and Weisberg, 1982). Influential cases were defined as observations with Cook's distance exceeding the predefined threshold (calculated as 4/N; N=number of observations (Bollen and Jackman, 1985)). In case observations exceeding the threshold were detected, analyses were rerun excluding those observations to test for the robustness of the results.

To account for the effect of amyloid pathology, the main analyses were repeated with regional amyloid-PET centiloid or tau-PET x amyloid-PET centiloid as additional predictors. All models were controlled for age, gender, diagnosis, education (fixed effects) and the study site as a random effect.

Next, we tested whether increased global or regional amyloid-PET was associated with reduced perfusion in DMN ROIs, i.e. predilection areas of amyloid deposition. To this end, we conducted mixed-effect regression analyses with global or regional amyloid-PET centiloid in DMN ROIs, as predictors of CBF in spatially corresponding ROIs. The analyses were repeated with regional tau-PET as additional predictor. All models were controlled for age, gender, diagnosis, education (fixed effects) and the study site as a random effect.

Lastly, we tested the associations between MRI markers of SVD (WMH volume and microbleeds) and global CBF. To that end, we used linear mixed-effect regression model with IHS-transformed WMH ratio or the microbleeds count as the independent variable and global mean CBF as the dependent variable, accounting for age, gender, diagnosis, education (fixed effects) and study site (random effect).

All analyses were performed using R statistical software package (http://www.R-project.org). Associations (standardized beta coefficients and correlation) were considered significant when meeting an α-threshold of 0.05. Correction for multiple comparisons was done using Bonferroni correction.

### 2.10. Data availability statement

Data on participant demographics are available in Table 1. ADNI data are accessible from http://adni.loni.usc.edu/data-samples/access-data/.

**Table 2**
Linear mixed models testing the regional effects of tau-PET on CBF in the whole group (n = 156)

| ROI | Tau | |
|---|---|---|
| | b/SE | *p*-value |
| Braak I | -0.371/0.088 | <0.001* |
| Braak III/IV | -0.120/0.089 | 0.180 |
| Braak V/VI | 0.156/0.082 | 0.057 |

Models are controlled for age, gender, education, diagnosis (fixed effects) and study site (random effect).
* Remains significant after applying a Bonferroni-corrected α-threshold of 0.017 (i.e., $\alpha = 0.05$ adjusted for 3 tests).

## 3. Results

### 3.1. Sample characteristics

For the current study, we analyzed data from 156 participants of the ADNI cohort, including 84 CN, 51 MCI and 21 AD dementia subjects (see Table 1 for sample characteristics). After correction for multiple comparisons, there were no differences in baseline demographics (age, gender, education) as well as in microbleeds count between the different diagnostic groups. As expected, AD dementia subjects had lower MMSE score, higher frequency of Aβ positivity and APOE ε4 carriage, higher global Aβ centiloid, higher global tau-PET SUVR, lower mean global CBF, and higher WMH volume.

Regional distributions of amyloid-PET centiloid, tau-PET SUVRs and CBF within the sample are shown for the Desikan-Kiliany ROIs in supplementary Figure 1.

### 3.2. Higher tau-PET is associated with lower perfusion exclusively in the entorhinal cortex

In a first step, we tested the hypothesis that tau pathology is associated with reduced perfusion in Braak stage ROIs (Figure 1A). As shown in Fig. 2 (Table 2), we found that higher tau-PET was associated with lower CBF in the entorhinal cortex (Braak I: $\beta = -0.371$, SE = 0.088, $p < 0.001$) accounting for confounding effects of age, gender, diagnosis, education (fixed effects) and study site (random effect). After exclusion of nine outliers detected based on Cook's distance, the association between tau-PET and CBF in the entorhi-

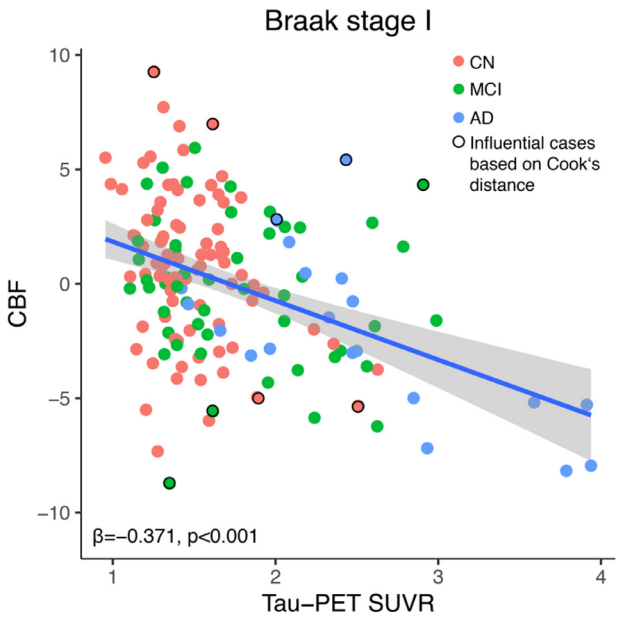


**Fig. 2.** Higher tau-PET is associated with lower CBF in the entorhinal cortex (Braak stage I).

nal cortex remained significant (Braak I: $\beta$ = -0.423, SE = 0.088, $p < 0.001$). There were no significant associations between tau-PET and CBF in Braak stage ROIs III/IV and V/VI ($p$ = 0.180 and $p$ = 0.057 respectively). The association in the entorhinal cortex remained significant after applying a Bonferroni-corrected $\alpha$-threshold of 0.017 (i.e., $\alpha$ = 0.05 adjusted for 3 tests).

To test whether the association between tau-PET and CBF in the entorhinal cortex is independent of A$\beta$, as a first step we split the sample into A$\beta$- and A$\beta$+ subgroups. We found significant associations both in the A$\beta$+ subgroup (Braak I: $\beta$ = -0.485, SE = 0.139, $p$ = 0.001), and the A$\beta$- subgroup (Braak I: $\beta$ = -0.313, SE = 0.095, $p$ = 0.002). Similarly, inclusion of regional amyloid-PET as a covariate in the main analysis did not alter the association between tau-PET and CBF in the entorhinal cortex (Braak I: $\beta$ = -0.363, SE = 0.095, $p < 0.001$). No interaction between regional tau-PET and regional amyloid-PET centiloid was observed.

To ensure that our results are not driven by extreme AD dementia cases, we repeated the analysis in a nondemented subgroup (consists of 84 CN and 51 MCI participants). We found that the association between higher tau-PET and lower CBF remained significant in the entorhinal cortex (Braak I: $\beta$ = -0.236, SE = 0.086, $p$ = 0.007).

As exploratory analysis we also tested the effect of APOE genotype on the association between tau-PET and CBF. Inclusion of APOE status as a covariate in the main analysis did not alter the association between tau-PET and CBF in the entorhinal cortex (Braak I: $\beta$ = -0.412, SE = 0.095, $p < 0.001$). We found a significant association of tau-PET and CBF, both in the APOE e4- non-carriers subgroups (Braak I: $\beta$ = -0.397, SE = 0.111, $p < 0.001$) as well as in the APOE e4+ carriers subgroup (Braak I: $\beta$ = -0.372, SE = 0.162, $p$ = 0.026). No interaction between regional tau-PET and APOE genotype was observed. See supplementary Table 1 for detailed statistics.

### 3.3. Higher global and regional amyloid-PET are associated with reduced perfusion in temporo-parietal regions

We tested whether CBF is associated with global or regional amyloid-PET centiloid in DMN ROIs (Fig. 1B). As shown in Fig. 3 (Table 3), higher global amyloid-PET centiloid was associated with lower CBF in the inferior temporal ($\beta$ = -0.367, SE = 0.083, $p < 0.001$), inferior parietal ($\beta$ = -0.259, SE = 0.076, $p < 0.001$), and precuneus ($\beta$ = -0.214, SE = 0.085, $p$ = 0.013). Associations in the inferior temporal and the inferior parietal remained significant after applying a Bonferroni-corrected $\alpha$-threshold of 0.008 (i.e., $\alpha$ = 0.05 adjusted for 6 tests). Similar results were observed when testing the associations between regional amyloid-PET centiloid and CBF.

**Table 3**
Linear mixed models testing the effects of global amyloid-PET on CBF in the amyloid subsample (n = 145)

| ROI | A$\beta$ | |
|---|---|---|
| | b/SE | $p$-value |
| Inferior temporal | -0.367/0.083 | <0.001* |
| Parahippocampus | -0.094/0.092 | 0.305 |
| Inferior parietal | -0.259/0.076 | <0.001* |
| Posterior cingulate | 0.041/0.087 | 0.637 |
| Precuneus | -0.214/0.085 | 0.013 |
| Medial orbitofrontal | -0.042/0.082 | 0.610 |

Models are controlled for age, gender, education, diagnosis (fixed effects) and study site (random effect).
* Remains significant after applying a Bonferroni-corrected $\alpha$-threshold of 0.008 (i.e., $\alpha$ = 0.05 adjusted for 6 tests).

When including in the model tau-PET obtained in the same ROIs, the association between global amyloid-PET centiloid and CBF remained unchanged in the inferior temporal and the precuneus. However, in the inferior parietal, global amyloid-PET centiloid no longer had a significant association with CBF, instead, an association between tau-PET and CBF ($\beta$ = -0.336, SE = 0.083, $p < 0.001$) was observed. See supplementary Table 2 for detailed statistics.

### 3.4. CBF is not associated with MRI markers of SVD

In order to ensure that our results are not driven by vascular factors, we tested the association between MRI markers of SVD (WMH volume and microbleeds) and CBF. No associations between global mean CBF and WMH volume ($p$ = 0.77) or microbleeds count ($p$ = 0.56) were observed.

## 4. Discussion

Our main findings show an association between higher tau-PET and lower CBF in the entorhinal cortex, independent of A$\beta$ pathology. For A$\beta$, higher global and regional amyloid-PET were associated with reduced CBF in temporo-parietal regions, even after controlling for tau-PET in the same ROIs. There were no associations between MRI-markers of SVD and CBF. Together, these results suggest that pathologic tau, is a major correlate of lower CBF in early Braak stages, independent of A$\beta$, SVD markers and APOE genotype.

Our dual-tracer assessment of A$\beta$ and tau pathology allowed to discern the roles of each pathology in local decreases in CBF. Our results provide an important advance beyond previous reports that focused only on the association between amyloid-PET and CBF (Bangen et al., 2017; Hansson et al., 2018; Mattsson et al., 2014; McDade et al., 2014; Michels et al., 2016; Rodell et al., 2016). Our results of the association between tau-PET and lower perfusion are in general agreement with previous findings on the association between higher levels of CSF biomarkers of tau and perfusion in cognitively normal APOE e4 carriers (Hays et al., 2020) and postmortem findings of higher Braak-stages of tau pathology to be associated with higher expression of the vascular endothelial

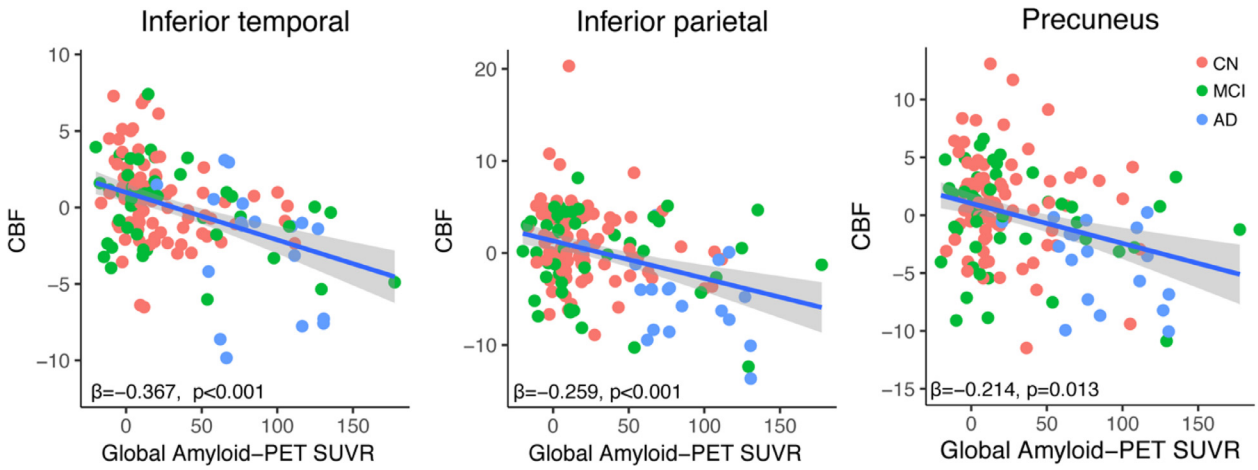


**Fig. 3.** Higher global amyloid-PET is associated with lower CBF in the inferior temporal, inferior parietal and precuneus.

growth factor (VEGF), i.e. a marker of hypoperfusion related hypoxia (Thomas et al., 2015). Interestingly, tau-PET was associated also with lower CBF in the inferior parietal in the secondary analysis focusing on predilection areas of A$\beta$, suggesting that also subtle elevations of tau-PET are related to lower perfusion. Together these findings suggest that local associations of tau-PET and CBF are strongest in the entorhinal cortex, but tau pathology may drive amyloid related changes in CBF also in other higher cortical areas.

We found associations between global as well as regional amyloid-PET and lower temporo-parietal perfusion. While our findings are in agreement with previous reports (Mattsson et al., 2014; Tosun et al., 2014), our results also suggest that for the attribution of CBF reductions to A$\beta$, tau pathology needs to be taken into account. As a note of caution, however, the current study design does not allow for a causative interpretation of any effects of tau pathology, and thus our findings neither address the directionality nor answer the question which specific pathology is causing CBF changes.

The mechanisms linking local tau pathology to local perfusion are not established yet. A potential candidate mechanism includes tau pathology to cause vascular changes that in turn lead to hypoperfusion. A recent study in transgenic mouse model of neurofibrillary tangles showed structural microvascular abnormalities and disrupted blood flow that was associated with neurodegeneration (Bennett et al., 2018). In brain tissue from both transgenic mice of tau pathology and brain tissue from AD patients, tau pathology was associated with alterations in RNA expression linked to vascular function and hypoxia. In contrast, those changes were not observed in a transgenic mouse model of A$\beta$ (Bennett et al., 2018). These observations in mice and humans suggest that tau pathology may directly impinge upon the microvasculature and thus reduced hypoperfusion. However, lower perfusion may also cause the pathologic tau accumulation as chronic hypoperfusion has been found to be associated with higher phosphorylated tau and A$\beta$ oligomers in rodents (Park et al., 2019). Yet, in nondemented elderly individuals with chronic hypoperfusion due to unilateral artery occlusion showed neither higher amyloid nor tau pathology, suggesting that hypoperfusion may not be eliciting AD pathology (Hansson et al., 2018). It should be noted though that the sample was small, with only 5 individuals receiving tau-PET, and thus the cause of events in humans remains to be established. A third possibility is that tau pathology causes GM atrophy which in turn reduces perfusion. However, other studies using combined structural MRI and ASL changes reported spatially divergent patterns of CBF reduction and GM atrophy in MCI and AD (Tosun et al., 2014; Wirth et al., 2017), supporting the view that CBF alterations do not occur merely as a function of neurodegeneration. In the current study, correction for PVE did not alter the results, thus, while the influence of GM atrophy on CBF changes cannot be excluded, it is unlikely that CBF changes can be reduced to GM atrophy.

Previous study reported increased tau-PET levels in subjects with SVD (Kim et al., 2018). Because SVD is associated with reduced cerebral perfusion (Shi et al., 2016), it is possible that any association between tau and lower perfusion is mediated due to SVD. However, we found no association between SVD markers and CBF in contrast to previous reports of an association between lower perfusion and higher number of microbleeds in nondemented elderlies (Gregg et al., 2015). A potential cause for the discrepancies in the findings is the relatively lower number of microbleeds in the current study compared to that in the previous study. For WMH, findings have been inconsistent, where the latter study reported no association between WMH and CBF (Gregg et al., 2015), but a positive association was reported in nondemented individuals in other studies (Kim et al., 2020). We note that there is currently no direct biomarker of SVD available, rather proxy measure such as WMH and microbleeds provide only crude measures of SVD in vivo. While we found no evidence supporting a role of SVD in the association between tau pathology and CBF, we cation that the current study was not tailored to test these associations. Moreover, since we focused only on grey matter perfusion, we cannot exclude the effect of SVD on perfusion in the white matter. Therefore, the role of SVD in tau associated decreases in perfusion in human remains to be tested.

Some limitations of this study should be considered. First, our study design was cross-sectional and not longitudinal, therefore we could not determine the temporal relationships between tau and CBF changes. Second, ADNI is a multi-site study and as such is susceptible to variability across sites. Therefore, we limited the current study to data acquired on a single scanner and all regression models were controlled for study site effects. Third, pCASL is currently the recommended ASL method by the ISMRM Perfusion Study Group and European Consortium for ASL in Dementia due to its relatively high signal-to-noise ratio (SNR) and clinical applicability (Alsop et al., 2015). However, the hemodynamic status of each individual cannot be precisely estimated using the current method and therefore the quantitative values of CBF may not be accurate. Optimizations of pCASL, such as multi-phase sequences, can collect data in multiple time phases and therefore may offer a more accurate CBF measure (Sugimori et al., 2015). Fourth, the sample size of the AD dementia group in our study was relatively small and most of the subjects were nondemented with

relatively low levels of tau-PET (Johnson et al., 2016; Jack et al., 2017). Enrichment of the sample with subjects with more advanced tau pathology, may have resulted in higher sensitivity to detect associations between CBF and tau-PET not only in the entorhinal cortex but also higher cortical areas. Lastly, we investigated only linear associations between CBF vs amyloid- or tau-PET. Previous studies reported - apart from decreases - also increases in CBF (Wierenga et al., 2012; Beason-Held et al., 2013; Fazlollahi et al., 2020), suggesting that changes in CBF are complex in AD. However, the results of those previous studies were inconsistent with regard to which specific brain regions and clinical phases are linked to increased CBF (Wierenga et al., 2014), and several studies did not report any increases in CBF in MCI (Binnewijzend et al., 2013; Wirth et al., 2017) or AD dementia (Chen et al., 2011; Binnewijzend et al., 2013) at all. In the current study, we observed only inverse associations between CBF and tau-PET or amyloid-PET. The current sample size did not allow to model nonlinear relationships or analyses stratified by clinical subgroup, and thus nonlinear relationships with tau-PET remain to be investigated.

## 5. Conclusion

In conclusion, decreases in regional CBF can be observed not only in an amyloid-PET manner but also tau-PET dependent, preferentially in regions of high tau-PET uptake. These associations are detectable at an early stage of tau pathology in the absence of clinical dementia as well as in later AD stages and are independent of A$\beta$ pathology, APOE genotype or SVD markers. Thus, CBF measured by pCASL could potentially identify tau- associated CBF alterations in preclinical phase and serve as a noninvasive biomarker for the early detection of AD.

## Declaration of competing interest

None.

## Author disclosures

Dr. Weiner served on Advisory Boards for Eli Lilly, Cerecin/Accera, Roche, Alzheon, Inc., Merck Sharp & Dohme Corp., Nestle/Nestec, PCORI/PPRN, Dolby Family Ventures, Brain Health Registry and ADNI. He serves on the Editorial Boards for Alzheimer's & Dementia and MRI. He has provided consulting and/or acted as a speaker/lecturer to Cerecin/Accera, Inc., Alzheimer's Drug Discovery Foundation (ADDF), Merck, BioClinica, Eli Lilly, Indiana University, Howard University, Nestle/Nestec, Roche, Genentech, NIH, Lynch Group GLC, Health & Wellness Partners, Bionest Partners, American Academy of Neurology (AAN), and Society for Nuclear Medicine and Molecular Imaging (SNMMI). He holds stock options with Alzheon, Inc.

## Acknowledgements

The study was supported by the German Center for Neurodegenerative Diseases (DZNE), Alzheimer Forschung Initiative (AFI, Grant 15035 to ME), LMUexcellent (to ME) and by the Deutsche Forschungsgemeinschaft (DFG, German Research Foundation) grant for major research instrumentation (DFG, INST 409/193-1 FUGG). ADNI data collection and sharing for this project was funded by the ADNI (National Institutes of Health Grant U01 AG024904) and DOD ADNI (Department of Defense award number W81XWH-12-2-0012). ADNI is funded by the National Institute on Aging, the National Institute of Biomedical Imaging, and Bioengineering, and through contributions from the following: AbbVie, Alzheimer's Association; Alzheimer's Drug Discovery Foundation; Araclon Biotech; BioClinica, Inc.; Biogen; Bristol-Myers Squibb Company; CereSpir, Inc.; Cogstate; Eisai Inc.; Elan Pharmaceuticals, Inc.; Eli Lilly and Company; EuroImmun; F. Hoffmann-La Roche Ltd and its affiliated company Genentech, Inc.; Fujirebio; GE Healthcare; IXICO Ltd.; Janssen Alzheimer Immunotherapy Research & Development, LLC.; Johnson & Johnson Pharmaceutical Research & Development LLC.; Lumosity; Lundbeck; Merck & Co., Inc.; Meso Scale Diagnostics, LLC.; NeuroRx Research; Neurotrack Technologies; Novartis Pharmaceuticals Corporation; Pfizer Inc.; Piramal Imaging; Servier; Takeda Pharmaceutical Company; and Transition Therapeutics. The Canadian Institutes of Health Research is providing funds to support ADNI clinical sites in Canada. Private sector contributions are facilitated by the Foundation for the National Institutes of Health (www.fnih.org).

Dr. Weiner receives support for his work from the following funding sources:

NIH, DOD, PCORI, California Dept. of Public Health, U. Michigan, Siemens, Biogen, Hillblom Foundation, Alzheimer's Association. He also receives support from Johnson & Johnson, Kevin and Connie Shanahan, GE, VUmc, Australian Catholic University, The Stroke Foundation, and the Veterans Administration.

## Author contributions

AR designed the study, conducted the analyses, interpreted the results and drafted the manuscript, DT analyzed the data and provided critical review of the manuscript, NF and JN provided critical review of the manuscript, LF processed the data, MW provided critical review of the manuscript, ME designed the study, interpreted the results and drafted the manuscript.

## Supplementary materials

Supplementary material associated with this article can be found, in the online version, at doi:10.1016/j.neurobiolaging.2021.02.003.

## References

Alsop, D.C., Detre, J.A., Golay, X., Günther, M., Hendrikse, J., Hernandez-Garcia, L., Lu, H., MacIntosh, B.J., Parkes, L.M., Smits, M., van Osch, M.J.P., Wang, D.J.J., Wong, E.C., Zaharchuk, G., 2015. Recommended implementation of arterial spin-labeled perfusion MRI for clinical applications: A consensus of the ISMRM perfusion study group and the European consortium for ASL in dementia. Magn Reson Med 73 (1), 102–116.

Asllani, I., Borogovac, A., Brown, T.R., 2008. Regression algorithm correcting for partial volume effects in arterial spin labeling MRI. Magn Reson Med 60 (6), 1362–1371.

Baker, S.L., Maass, A., Jagust, W.J., 2017. Considerations and code for partial volume correcting [(18)F]-AV-1451 tau PET data. Data in Brief 15, 648–657.

Bangen, K.J., Clark, A.L., Edmonds, E.C., Evangelista, N.D., Werhane, M.L., Thomas, K.R., Locano, L.E., Tran, M., Zlatar, Z.Z., Nation, D.A., Bondi, M.W., Delano-Wood, L., 2017. Cerebral blood flow and amyloid-beta interact to affect memory performance in cognitively normal older adults. Front Aging Neurosci 9, 181.

Beason-Held, L.L., Goh, J.O., An, Y., Kraut, M.A., O'Brien, R.J., Ferrucci, L., Resnick, S.M., 2013. Changes in brain function occur years before the onset of cognitive impairment. J Neurosci 33 (46), 18008–18014.

Bennett, R.E., Robbins, A.B., Hu, M., Cao, X., Betensky, R.A., Clark, T., Das, S., Hyman, B.T., 2018. Tau induces blood vessel abnormalities and angiogenesis-related gene expression in P301L transgenic mice and human Alzheimer's disease. Proc Natl Acad Sci U S A 115 (6), E1289–E1E98.

Binnewijzend, M.A., Benedictus, M.R., Kuijer, J.P., van der Flier, W.M., Teunissen, C.E., Prins, N.D., Wattjes, M.P., van Berckel, B.N., Scheltens, P., Barkhof, F., 2016. Cerebral perfusion in the predementia stages of Alzheimer's disease. Eur Radiol 26 (2), 506–514.

Binnewijzend, M.A., Kuijer, J.P., Benedictus, M.R., van der Flier, W.M., Wink, A.M., Wattjes, M.P., van Berckel, B.N., Scheltens, P., Barkhof, F., 2013. Cerebral blood flow measured with 3D pseudocontinuous arterial spin-labeling MR imaging in Alzheimer disease and mild cognitive impairment: a marker for disease severity. Radiology 267 (1), 221–230.

Bollen, K.A., Jackman, R.W., 1985. Regression diagnostics: an expository treatment of outliers and influential cases. Sociolog Methods Res 13 (4), 510–542.

Bradley, K.M., O'Sullivan, V.T., Soper, N.D.W., Nagy, Z., King, E.M.F., Smith, A.D., Shepstone, B.J., 2002. Cerebral perfusion SPET correlated with Braak pathological stage in Alzheimer's disease. Brain 125 (8), 1772–1781.
Caballero, M.ÁA., Song, Z., Rubinski, A., Duering, M., Dichgans, M., Park, D.C., Ewers, M., 2020. Age-dependent amyloid deposition is associated with white matter alterations in cognitively normal adults during the adult life span. Alzheimer's Dementia n/a(n/a.
Chao, L.L., Buckley, S.T., Kornak, J., Schuff, N., Madison, C., Yaffe, K., Miller, B.L., Kramer, J.H., Weiner, M.W., 2010. ASL perfusion MRI predicts cognitive decline and conversion from MCI to dementia. Alzheimer Dis Assoc Disord 24 (1), 19–27.
Chen, Y., Wolk, D.A., Reddin, J.S., Korczykowski, M., Martinez, P.M., Musiek, E.S., Newberg, A.B., Julin, P., Arnold, S.E., Greenberg, J.H., Detre, J.A., 2011. Voxel-level comparison of arterial spin-labeled perfusion MRI and FDG-PET in Alzheimer disease. Neurology 77 (22), 1977–1985.
Cook, R.D., Weisberg, S., 1982. Residuals and influence in regression. Chapman and Hall, New York.
Desikan, R.S., Ségonne, F., Fischl, B., Quinn, B.T., Dickerson, B.C., Blacker, D., Buckner, R.L., Dale, A.M., Maguire, R.P., Hyman, B.T., Albert, M.S., Killiany, R.J., 2006. An automated labeling system for subdividing the human cerebral cortex on MRI scans into gyral based regions of interest. NeuroImage 31 (3), 968–980.
Fazlollahi, A., Calamante, F., Liang, X., Bourgeat, P., Raniga, P., Dore, V., Fripp, J., Ames, D., Maters, C.L., Rowe, C.C., Connelly, A., Villemagne, V.L., Salvado, O.Australian Imaging Biomarkers and Lifestyle (AIBL) Research Group, 2020. Increased cerebral blood flow with increased amyloid burden in the preclinical phase of alzheimer's disease. J Magn Reson Imaging 51 (2), 505–513.
Gregg, N.M., Kim, A.E., Gurol, M.E., Lopez, O.L., Aizenstein, H.J., Price, J.C., Mathis, C.A., James, J.A., Snitz, B.E., Cohen, A.D., Kamboh, M.I., Minhas, D., Weissfeld, L.A., Tamburo, E.L., Klunk, W.E., 2015. Incidental cerebral microbleeds and cerebral blood flow in elderly individuals. JAMA Neurol 72 (9), 1021–1028.
Habert, M.-O., de Souza, L.C., Lamari, F., Daragon, N., Desarnaud, S., Jardel, C., Dubois, B., Sarazin, M., 2010. Brain perfusion SPECT correlates with CSF biomarkers in Alzheimer's disease. Eur J Nuclear Med Mol Imaging 37 (3), 589–593.
Hansson, O., Palmqvist, S., Ljung, H., Cronberg, T., van Westen, D., Smith, R., 2018. Cerebral hypoperfusion is not associated with an increase in amyloid $\beta$ pathology in middle-aged or elderly people. Alzheimer's Dementia 14 (1), 54–61.
Hays, C.C., Zlatar, Z.Z., Meloy, M.J., Osuna, J., Liu, T.T., Galasko, D.R., Wierenga, C.E., 2020. Anterior cingulate structure and perfusion is associated with cerebrospinal fluid tau among cognitively normal older adult APOEvarepsilon4 carriers. J Alzheimer's Dis 73 (1), 87–101.
Jr. Jack Jr., C.R., Wiste, H.J., Schwarz, C.G., Lowe, V.J., Senjem, M.L., Vemuri, P., Weigand, S.D., Therneau, T.M., Knopman, D.S., Gunter, J.L., Jones, D.T., Graff-Radford, J, Kantarci, K., Roberts, R.O., Mielke, M.M., Machulda, M.M., Petersen, R.C., 2018. Longitudinal tau PET in ageing and Alzheimer's disease. Brain 141 (5), 1517–1528.
Jr. Jack Jr., C.R., Wiste, H.J., Weigand, S.D., Therneau, T.M., Lowe, V.J., Knopman, D.S., Gunter, J.L., Senjem, M.L., Jones, D.T., Kantarci, K., Machulda, M.M., Mielke, M.M., Roberts, R.O., Vemuri, P, Reyes, D.A., Petersen, R.C., 2017. Defining imaging biomarker cut points for brain aging and Alzheimer's disease. Alzheimer's Dementia 13 (3), 205–216.
Jagust, W.J., Landau, S.M., Koeppe, R.A., Reiman, E.M., Chen, K., Mathis, C.A., Price, J.C., Foster, N.L., Wang, A.Y., 2015. The ADNI PET Core: 2015. Alzheimer's & dementia: the journal of the. Alzheimer's Assoc 11 (7), 757–771.
Johnson, K.A., Schultz, A., Betensky, R.A., Becker, J.A., Sepulcre, J., Rentz, D., Mormino, E., Chhatwal, J., Amariglio, R., Rapp, K., Marshall, G., Albers, M., Mauro, S., Pepin, L., Alverio, J., Judge, K., Philiossaint, M., Shoup, T., Yokell, D., Dickerson, B., Gomez-Isla, T., Hyman, B., Vasdev, N., Sperling, R., 2016. Tau PET imaging in aging and early Alzheimer's disease. Ann Neurol 79 (1), 110–119.
Kim, C.M., Alvarado, R.L., Stephens, K., Wey, H.Y., Wang, D.J.J., Leritz, E.C., Salat, D.H., 2020. Associations between cerebral blood flow and structural and functional brain imaging measures in individuals with neuropsychologically defined mild cognitive impairment. Neurobiol Aging 86, 64–74.
Kim, H.J., Park, S., Cho, H., Jang, Y.K., San Lee, J., Jang, H., Kim, Y., Kim, K.W., Ryu, Y.H., Choi, J.Y., Moon, S.H., Weiner, M.W., Jagust, W.J., Rabinovici, G.D., DeCarli, C., Lyoo, C.H., Na, D.L., Seo, S.W., 2018. Assessment of extent and role of tau in subcortical vascular cognitive impairment using 18F-AV1451 positron emission tomography imaging. JAMA Neurol 75 (8), 999–1007.
Landau, S.M., Mintun, M.A., Joshi, A.D., Koeppe, R.A., Petersen, R.C., Aisen, P.S., Weiner, M.W., Jagust, W.J., 2012. Amyloid deposition, hypometabolism, and longitudinal cognitive decline. Ann Neurol 72 (4), 578–586.
Love, S., Miners, J.S., 2016. Cerebrovascular disease in ageing and Alzheimer's disease. Acta Neuropathol 131 (5), 645–658.
Maass, A., Landau, S., Baker, S.L., Horng, A., Lockhart, S.N., La Joie, R., Rabinovici, G.D., Jagust, W.J., 2017. Comparison of multiple tau-PET measures as biomarkers in aging and Alzheimer's disease. Neuroimage 157, 448–463.
Marquie, M., Normandin, M.D., Vanderburg, C.R., Costantino, I.M., Bien, E.A., Rycyna, L.G., Klunk, W.E., Mathis, C.A., Ikonomovic, M.D., Debnath, M.L., Vadev, N., Dickerson, B.C., Gomperts, S.N., Growdon, J.H., Johnson, K.A., Frosch, M.P., Hyman, B.T., Gomez-Isla, T., 2015. Validating novel tau positron emission tomography tracer [F-18]-AV-1451 (T807) on postmortem brain tissue. Ann Neurol 78 (5), 787–800.
Jr. Mattsson, N., Tosun, D., Insel, P.S., Simonson, A., Jack, C.R., Beckett, L.A., Donohue, M., Jagust, W., Schuff, N., Weiner, M.W.Alzheimer's Disease Neuroimaging Initiative, 2014. Association of brain amyloid-$\beta$ with cerebral perfusion and structure in Alzheimer's disease and mild cognitive impairment. Brain 137, 1550–1561 (Pt 5).
McDade, E., Kim, A., James, J., Sheu, L.K., Kuan, DC-H., Minhas, D., Gianaros, P.J., Ikonomovic, S., Lopez, O., Snitz, B., Price, J., Becker, J., Mathis, C., Klunk, W., 2014. Cerebral perfusion alterations and cerebral amyloid in autosomal dominant Alzheimer disease. Neurology 83 (8), 710.
Michels, L., Warnock, G., Buck, A., Macauda, G., Leh, S.E., Kaelin, A.M., Riese, F., Meyer, R., O'Gorman, R., Hock, C., Kollias, S., Gietl, A.F., 2016. Arterial spin labeling imaging reveals widespread and Abeta-independent reductions in cerebral blood flow in elderly apolipoprotein epsilon-4 carriers. J Cerebral Blood Flow Metab 36 (3), 581–595.
Mutsaerts, H.J.M.M., Petr, J., Groot, P., Vandemaele, P., Ingala, S., Robertson, A.D., Václavů, L., Groote, I., Kuijf, H., Zelaya, F., O'Daly, O., Hilal, S., Wink, A.M., Kant, I., Caan, M.W.A., Morgan, C., de Bresser, J., Lysvik, E., Schrantee, A., Bjørnebekk, A., Clement, P., Shirzadi, Z., Kuijer, J.P.A., Wottschel, V., Anazodo, U.C., Pajkrt, D., Richard, E., Bokkers, R.P.H., Reneman, L., Masellis, M., Günther, M., MacIntosh, B.J., Achten, E., Chappell, M.A., van Osch, M.J.P., Golay, X., Thomas, D.L., De Vita, E., Bjørnerud, A., Nederveen, A., Hendrikse, J., Asllani, I., Barkhof, F., 2020. ExploreASL: An image processing pipeline for multi-center ASL perfusion MRI studies. NeuroImage 219, 117031.
Palmqvist, S., Schöll, M., Strandberg, O., Mattsson, N., Stomrud, E., Zetterberg, H., Blennow, K., Landau, S., Jagust, W., Hansson, O., 2017. Earliest accumulation of $\beta$-amyloid occurs within the default-mode network and concurrently affects brain connectivity. Nat Commun 8 (1), 1214.
Park, J.H., Hong, J.H., Lee, S.W., Ji, H.D., Jung, J.A., Yoon, K.W., Lee, J.I., Won, K.S., Song, B.I., Kim, H.W., 2019. The effect of chronic cerebral hypoperfusion on the pathology of Alzheimer's disease: A positron emission tomography study in rats. Sci Rep 9 (1), 14102.
Petersen, R.C., Aisen, P.S., Beckett, L.A., Donohue, M.C., Gamst, A.C., Harvey, D.J., Jack, C.R., Jagust, W.J., Shaw, L.M., Toga, A.W., Trojanowski, J.Q., Weiner, M.W., 2010. Alzheimer's Disease Neuroimaging Initiative (ADNI): clinical characterization. Neurology 74 (3), 201–209.
Petr, J., Mutsaerts, H.J.M.M., De Vita, E., Steketee, R.M.E., Smits, M., Nederveen, A.J., Hofheinz, F., van den Hoff, J., Asllani, I, 2018. Effects of systematic partial volume errors on the estimation of gray matter cerebral blood flow with arterial spin labeling MRI. Magnetic Resonance Materials in Physics. Biol Med 31 (6), 725–734.
Rodell, A.B., O'Keefe, G., Rowe, C.C., Villemagne, V.L., Gjedde, A., 2016. Cerebral blood flow and a beta-amyloid estimates by WARM analysis of [(11)C]PiB uptake distinguish among and between neurodegenerative disorders and aging. Front Aging Neurosci 8, 321.
Shi, Y., Thrippleton, M.J., Makin, S.D., Marshall, I., Geerlings, M.I., de Craen, A.J.M., van Buchem, M.A., Wardlaw, J.M., 2016. Cerebral blood flow in small vessel disease: A systematic review and meta-analysis. J Cerebral Blood Flow Metab 36 (10), 1653–1667.
Stomrud, E., Forsberg, A., Hägerström, D., Ryding, E., Blennow, K., Zetterberg, H., Minthon, L., Hansson, O., Londos, E., 2012. CSF biomarkers correlate with cerebral blood flow on SPECT in healthy elderly. Dement Geriatric Cognit Disord 33 (2–3), 156–163.
Sugimori, H., Fujima, N., Suzuki, Y., Hamaguchi, H., Sakata, M., Kudo, K., 2015. Evaluation of cerebral blood flow using multi-phase pseudo continuous arterial spin labeling at 3-tesla. Magn Reson Imaging 33 (10), 1338–1344.
Thomas, T., Miners, S., Love, S., 2015. Post-mortem assessment of hypoperfusion of cerebral cortex in Alzheimer's disease and vascular dementia. Brain 138, 1059–1069 (Pt 4).
Tosun, D., Joshi, S., Weiner, M.W.Alzheimer's Disease Neuroimaging Initiative, 2014. Multimodal MRI-based imputation of the Abeta+ in early mild cognitive impairment. Ann Clin Transl Neurol 1 (3), 160–170.
Tosun, D., Schuff, N., Rabinovici, G.D., Ayakta, N., Miller, B.L., Jagust, W., Kramer, J., Weiner, M.M., Rosen, H.J., 2016. Diagnostic utility of ASL-MRI and FDG-PET in the behavioral variant of FTD and AD. Ann Clin Transl Neurol 3 (10), 740–751.
Wierenga, C.E., Dev, S.I., Shin, D.D., Clark, L.R., Bangen, K.J., Jak, A.J., Rissman, R.A., Liu, T.T., Salmon, D.P., Bondi, M.W., 2012. Effect of mild cognitive impairment and APOE genotype on resting cerebral blood flow and its association with cognition. J Cerebral Blood Flow Metab 32 (8), 1589–1599.
Wierenga, C.E., Hays, C.C., Zlatar, Z.Z., 2014. Cerebral blood flow measured by arterial spin labeling MRI as a preclinical marker of Alzheimer's disease. J Alzheimer's Dis 42 (Suppl 4), S411–S419.
Wirth, M., Pichet Binette, A., Brunecker, P., Kobe, T., Witte, A.V., Floel, A., 2017. Divergent regional patterns of cerebral hypoperfusion and gray matter atrophy in mild cognitive impairment patients. J Cerebral Blood Flow Metab 37 (3), 814–824.
Wolf, R.L., Detre, J.A., 2007. Clinical neuroimaging using arterial spin-labeled perfusion magnetic resonance imaging. Neurotherapeutics 4 (3), 346–359.
Wolters, F.J., Zonneveld, H.I., Hofman, A., van der Lugt, A., Koudstaal, P.J., Vernooij, M.W., Ikram, M.A.Heart-Brain Connection Collaborative Research Group, 2017. Cerebral perfusion and the risk of dementia: a population-based study. Circulation 136 (8), 719–728.
Xekardaki, A., Rodriguez, C., Montandon, M.L., Toma, S., Tombeur, E., Herrmann, F.R., Zekry, D., Lovbald, K.O., Barkhof, F., Giannakopoulos, P., Haller, S., 2015. Arterial spin labeling may contribute to the prediction of cognitive deterioration in healthy elderly individuals. Radiology 274 (2), 490–499.
Yew, B., Nation, D.A., 2017. Alzheimer's Disease Neuroimaging I. Cerebrovascular resistance: effects on cognitive decline, cortical atrophy, and progression to dementia. Brain 140 (7), 1987–2001.